ORIGINAL RESEARCH

Coral-shaped tin oxide incorporated graphitic carbon nitride nanosheets as peroxidase mimic for sensitive colorimetric and fluorescence quenching based detection of hydrogen peroxide

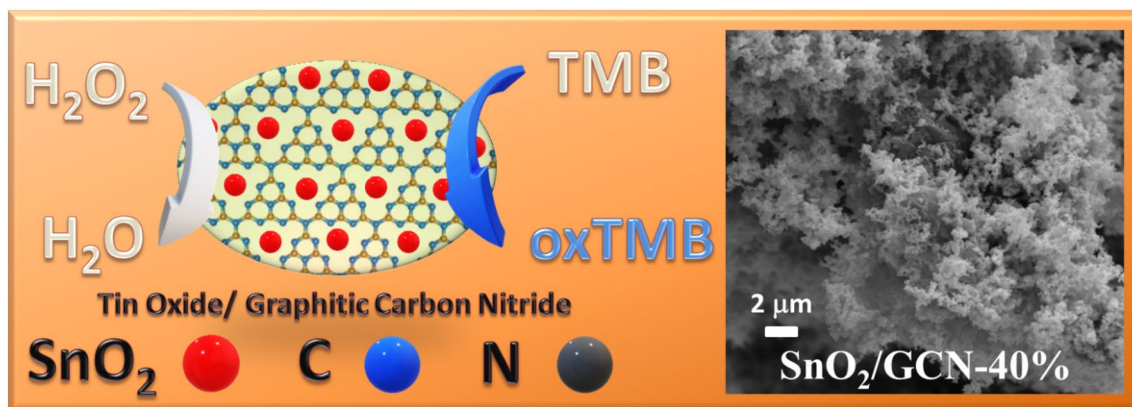Aftab Ahmed[1,2] · Akhtar Hayat[1] · Peter John[2] · Mian Hasnain Nawaz[1] · Muhammad Nasir[1]

Abstract

The enhanced peroxidase-like catalytic activity of coral-shaped graphitic carbon nitride (GCN) incorporated with tin oxide (SnO_2) is here reported and applied for the sensitive and selective colorimetric detection of hydrogen peroxide (H_2O_2). The SnO_2/GCN catalyzed the oxidation of 3, 3′, 5, 5′-tetramethylbenzidine, and H_2O_2 which resulted in the appearance/change of color in the visible range. The results of peroxidase-like activity showed that the growth of SnO_2 on GCN nanosheets improved structure, optical, and electronic properties considerably. SnO_2/GCN-40% showed the best activity because of the optimal loading of SnO_2, unique structural, electronic, optical, and electrical properties. The catalytic reaction of coral-shaped SnO_2/GCN-40% followed the typical Michaelis–Menten equation, and the affinity of coral-shaped SnO_2/GCN-40% to TMB and H_2O_2 was higher than that of horseradish peroxide. The present study showed a rapid, selective, and sensitive response toward the H_2O_2 bioassay in a linear range of $10-655$ μM with a limit of detection of 0.3 μM (S/N ratio of 3). The study may provide a promising method of performance improvement for applications in catalysis, biosensors, and nanomaterial-engineering fields.

Graphical abstract

Scheme shows the interaction of tin oxide with graphitic carbon nitride which resulted in a coral-shaped structure shown in SEM image. It also shows the interaction of tin oxide and graphitic carbon nitride with H_2O_2 in the presence of TMB (3,3′, 5,5′-Tetramethylbenzidine) and as a consequence, TMB gets oxidized and ended up in change in color.

✉ Muhammad Nasir
muhammadnasir@cuilahore.edu.pk

Extended author information available on the last page of the article

Introduction

The use of Hydrogen Peroxide (H_2O_2) is recently quite prevalent in food processing, household, and industrial applications such as the preparation of disinfectants, pharmaceuticals, and industrial bleaches. Also, it is known to be the cause of the different activities in the human body such as aging, cancer, diabetes, cardiovascular diseases, and tissue-damaging [1]. Therefore, its detection and monitoring are highly desirable to avoid or reduce its ill effects on our body. In the past, H_2O_2 concentration was determined through the absorbance measurement of the H_2O_2 molecules at 240 nm [2]. A variety of methods was also reported, including high-performance-liquid-chromatography (HPLC) [3], titrimetric [4], colorimetric, fluorescence [5], luminescence [6], chemiluminescence [7], electrochemical, and photoelectrochemical methods [8]. Among these detections methods, the colorimetric method has offered advantages like simplicity, low-cost, fast-response, high-sensitivity, and high-selectivity in operation. Natural enzymes like horseradish peroxide were also reported for determining H_2O_2 [9]. Enzymatic detection of H_2O_2 was sensitive and selective, but the sensing procedure has many limitations related to the properties of the enzymes. Natural enzymes are denatured at high pH and temperature. Natural enzymes preparation and purification is costly, complicated, and involves many steps [10]. Nanomaterials are used as artificial enzymes because of their enzyme-like characteristics to solve natural enzymes related problems in sensing [11]. These artificial enzymes of nanomaterials are termed as nanozymes [12].

Under such a context, nanozymes are an efficient candidate for the active layer in the colorimetric sensor development because of remarkable properties. Graphitic carbon nitride (GCN) can be used for designing a sensor once this material becomes capable of hosting active agents. GCN is a carbon-based two-dimensional semiconductor nanomaterial. It can be prepared easily from the low-cost nitrogen-rich precursors. However, GCN has some intrinsic drawbacks like low surface area, a high rate of electron–hole pair's recombination, and poor conductivity. These intrinsic drawbacks of GCN have limited its applications in fields like sensors and biosensors. These drawbacks of GCN can be improved by nanostructuring [13], surface functionalization, elemental doping, and combining with organic polymers [14], metal–organic frameworks, metals [15], and metal oxides [16, 17]. Recently, metal oxides and their nanocomposites such as MoO_3 [18], porous carbon [19], NiO [20], CoO [21], V_2O_3 [22], MnO_2 [23–25], Co_3O_4 [26], metal nanoclusters [27] and noble metal nanostructures [28] are found as artificial enzymes. So, the combination of GCN with metal oxide can improve its structural, electronic, optical, and electrical properties [29]. Some of the improved properties include the high light-absorption ability [30], surface area [31], conductivity, electron-transferability [32], and low charge carriers recombination's rate [33]. These factors support GCN/metal oxide combinations as an ideal active materials for the sensor development.

Herein, we report the development of an optical-colorimetric sensor for H_2O_2 determination using novel coral-shaped GCN nanocomposites with SnO_2. The coral-shaped GCN/SnO_2 composites are prepared from different ratios of GCN and SnO_2 using an ultrasonic-assisted deposition strategy. The SnO_2/GCN-40% nanocomposite has shown the advantages like simplicity in operation, unique structure, better optical and electronic properties as compared to the single nanomaterials. A color change was found, when the suspensions of prepared samples were added in 3, 3′, 5, 5′-tetramethylbenzidine (TMB) in the presence of H_2O_2 in the colorimetric bioassay. The intensity of color change was depended upon the peroxidase-like catalytic activity of the samples. The coral-shaped SnO_2/GCN-40% showed the highest color change in the colorimetric H_2O_2 assay and the highest peroxidase-like activity as compared to the rest of the synthesized samples. Therefore, as a result of the higher peroxidase-like activity of coral-shaped SnO_2/GCN-40% NSs, it was selected for further practical, visual, and colorimetric assays of H_2O_2 detection. H_2O_2 detection by using novel coral-shaped SnO_2/GCN Nanosheets has offered advantages of low-cost, simplicity, rapid response, and high sensitivity. The H_2O_2 sensor fabrication, designing, and reaction mechanisms are displayed in Scheme 1.

Materials and methods

Materials

Melamine, pyrocatechol, sodium hydroxide, sodium chloride, potassium chloride, calcium chloride, dopamine, and TMB (99.6%) were purchased from Sigma-Aldrich, United Kingdom. L(+)-ascorbic acid, commercially pure tin (IV) oxide powder (SnO_2) were received from Daejung Chemical and Metals Co Ltd, Korea. Anhydrous sodium acetate, uric acid, potassium dichromate, sodium hypochlorite pentahydrate, phosphoric acid (H_3PO_4, 85% of w/w), and hydrochloric acid (HCl, 36.5–38% ACS grade) were obtained from BDH Chemicals, England. Acetic acid, L-cysteine, and hydrogen peroxide (H_2O_2, 30% of w/v) were received from Merck, Germany. Dimethyl sulfoxide (DMSO), and ethanol (> 99.8%) were purchased from the RCI Labscan Ltd, Thailand. Rhodamine B (RhB) was obtained from Avonchem Ltd, United Kingdom. Phosphate buffer saline tablets (PBS, 10 mM, pH 7.3–7.5, biotechnology grade) were collected
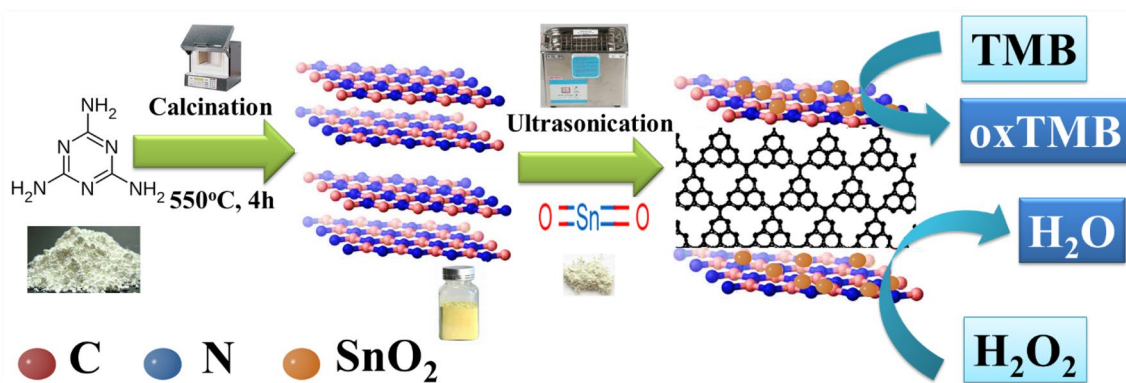
Scheme 1 Schematic representation of the synthesis protocol and H_2O_2 determination by SnO_2/GCN-40% Nanosheets catalyzed reaction

from VWR International Ltd, USA. Analytical grade chemicals and reagents were used as received. During experimentation, solutions were prepared in deionized water of conductivity less than 22 $\mu\Omega$ cm^{-1} from an Elga-Ultra-Pure deionizer.

Instruments

Surface morphology and shape characteristics of the samples are studied using electron microscopy. Scanning electron microscope (SEM) high-resolution images of the samples were obtained on a TESCAN Vega-3 LMU SEM at 10 kV. Elemental profile and purity analysis of the samples were performed by using a powerful technique of energy-dispersive X-rays (EDX) on the SEM. X-ray diffraction (XRD) study of the as-prepared samples was done on the Rigaku-D/max-2500 powder X-ray diffractometer. XRD PC system was equipped with a graphitic monochromator, and a copper targeted x-ray tube was used to generate Nickel filtered Copper (Kα) radiations. Fourier transform infrared (FTIR) spectroscopy is used to find the functional groups in the samples. FTIR spectra of the samples were recorded by using the Nicolet 6700 Thermo Fisher Scientific FTIR spectrophotometer. FTIR spectrum was scanned in attenuated total reflectance mode using eight cm^{-1} of resolution. For determination of the bandgap and absorption edge of the powdered samples, ultraviolet–visible (UV–Vis) diffuse reflectance spectra (DRS) were obtained on a Perkin Elmer Lambda 35 spectrophotometer under ambient temperature conditions. Samples were filled and pressed into a tablet in a disc of barium sulfate before putting in the holder for UV–Vis DRS analysis. The composition, phase information, interaction, and structural disorder in the samples are studied by using Raman and Photoluminescence (PL) spectroscopy. Raman and PL spectra of the samples were obtained on Renishaw InVia integrated laser scanning confocal microscope (U.K), which was equipped with a laser excitation source of

wavelength 457 nm (nm). The PL analysis of the samples was performed at a laser exposure time of ten seconds, laser power of 0.1%, a grating of 1800 I min^{-1}, and an objective of 5x. The size distribution of nanoparticles in the suspensions of the samples are determined using a dynamic light scattering (DLS) analysis. A BT-90 better size instrument was used for DLS analysis. The quantity of color substances in the reaction mixture is measured through the colorimetric analysis. The colorimetric analysis of the reaction mixtures was performed on a UV–Vis double-beam-spectrophotometer (Perkin Elmer Lambda 25) containing two quartz cuvette with each capacity of three millilitre (mL). UV–Vis absorption spectrum is used to find the effect of analyte concentrations on the change of absorption peak intensity and wavelength of maximum absorption (λmax) of the absorbing species in the reaction system. The absorption spectrum of the reaction mixtures was recorded in the wavelength range from 400 to 800 nm using a bandwidth setting of one nm at a wavelength scan rate of 960 nm min^{-1}. The fluorescence emission spectrum of the reaction mixtures was recorded on Agilent Carry Eclipse Fluoresce Spectrophotometer (USA).

Preparation of GCN

The GCN was prepared by the direct pyrolysis of precursor in ceramic crucible covered with ceramic lid [34]. More specifically, Melamine (10 g) was placed in the semi-covered ceramic crucible (100 mL) and heated in the muffle furnace to 550 °C using a temperature ramp of 5 °C min^{-1} under atmospheric air conditions, and then maintained this temperature for four hours. After cooling the furnace, the yellow product was obtained, which was washed with distilled water three times to take out any impurities and the unreacted nitrogenous materials. The final product was dried at 60 °C for ten hours and labeled as GCN.

Preparation of SnO$_2$/GCN nanocomposites

The SnO$_2$/GCN nanocomposites were prepared through the ultrasonic-assisted deposition method at room temperature [35]. The energy of ultrasonic-waves formed the structure of SnO$_2$/GCN nanocomposites through the dispersion of GCN and SnO$_2$. In a typical procedure, different amount of GCN (300, 270, 240, 210, 180, 150, 120, 90, 60, 30, and 0 mg) were mixed with SnO$_2$ (0, 30, 60, 90, 120, 150, 180, 210, 240, 270, and 300 mg) in 20 mL glass vials containing 10 mL methanol. The mixture in the vials was placed in the sonicator bath for 10 min to stick SnO$_2$ on the dispersed GCN nanosheets. The vials containing the samples were placed in the fume hood for 24 h. Later, the product was dried in the vacuum oven at 60 °C overnight to remove the methanol. The final products were ground for 5 min in mortar and pestle to homogenize the mixture and generally labeled as SnO$_2$/GCN-x%, where x (0, 10, 20, 30, 40, 50, 60, 70, 80, 90, and 100) was the weight percentages of SnO$_2$ about GCN in the products.

Colorimetric analysis

The peroxidase-like activity of the as-prepared samples was determined using the dispersion of solid samples. The dried samples were dispersed into two-dimensional nanostructures in deionized water using the ultra-sonication method [36]. Generally, 2 mg of the dried samples were added in the 2 mL of the distilled water and bath ultrasonicated for 10 min at room temperature. These prepared nanosheets suspensions were used for the reaction between visualizing reagent (TMB) and H$_2$O$_2$. The 46.75 μL of nanosheets suspension (1 mg mL^{-1}) was mixed into 2810 μL of sodium acetate buffer (pH 5, 100 mM) in a shaker for 1 min. Then, 45 μL of TMB (20 mM in DMSO) and 98.25 μL of H$_2$O$_2$ (20 mM in distilled water) were added to the above reaction mixture. The final concentrations in the reaction mixture were 15.58 μg mL^{-1} of sample NSs, 300 μM of TMB, and 655 μM of the H$_2$O$_2$. Because of the reaction between H$_2$O$_2$, TMB, and sample NSs, the colour of the reaction mixture was changed to blue. This blue color of the reaction mixture was because of the oxidized TMB (oxTMB), which provided a prominent absorption peak at 654 nm in the absorption spectrum corresponding intensity of A$_{654}$ nm. The A$_{654}$ nm depended upon the catalyst concentration, pH of the buffer, temperature, and substrate concentrations (TMB or H$_2$O$_2$). Thats why the catalytic measurements were required to optimize before the final H$_2$O$_2$ detection. The optimal values of reaction conditions were determined by varying amount of SnO$_2$ in nanocomposites (0–100%), temperature (10–70 °C), pH (2.0–11.0), amount of catalyst (0–1000 μg mL^{-1}), time (0 − 30 min), TMB concentration (0–800 μM), and H$_2$O$_2$ concentration (0–7000 μM) in

sodium acetate buffer (100 mM). The procedure for sensor selectivity and NSs recyclability determination was the same as H$_2$O$_2$ detection, except that some other coexisting interfering compounds were added during selectivity study. The colloidal suspensions of the samples were stored in the refrigerator at 4 °C for further use. The colloidal suspensions of the samples were extremely stable and no sediments were appeared after several months of the preparation.

Steady-state kinetics of the reaction were found by determining the A$_{654}$ nm with respect to reaction time at optimum reaction conditions. The mechanism of the reaction were found by varying concentration of one substrate and taking concentration of other substrate constant. The reaction initial velocities were determined from the slope of the linear ranges of the initial reaction rates of kinetics curves. Steady-state kinetics constant (K$_m$ and V$_{max}$) were calculated by using Line-weaver-Burk plots of (1/velocity) against (1/ [substrate]) of the double reciprocal of Michaelis–Menten-equation,

$$V = \frac{V_{max} \times [S]}{K_m + [S]}$$

where K$_m$ was Michaelis–Menten constant, [S] was the concentration of the substrate and V and V$_{max}$ were velocities of the reaction.

Fluorescence analysis

To confirm the catalytic activity of coral-shaped SnO$_2$/GCN-40% NSs, fluorometric analysis was performed. First, a pre-scan of the RhB solution (70 ng mL^{-1}) was obtained. Then, the fluorescence emission spectrum of the reaction mixture (3 mL) containing 2855 μL of RhB (73.6 ng mL^{-1}) and 98.25 μL of H$_2$O$_2$ (20 mM) in the presence and absence of 46.75 μL of nanocomposite NSs (1 mg mL^{-1}) was scanned at an excitation of 554 nm. The 3 mL of the reaction mixture was contained 655 μM of H$_2$O$_2$, 15.58 μg mL^{-1} of NSs catalyst, and 70 ng mL^{-1} of RhB dye. The PBS solution (10 mM, pH 7.4) was used in each fluorescence measurement. Every time fresh H$_2$O$_2$ and RhB solution was prepared for each analysis.

Results and discussion

Characterization

The morphology and structure of the GCN, SnO$_2$/GCN, and SnO$_2$ were investigated through SEM micrographs and samples SEM images are displayed in Fig. 1a. SEM images of GCN showed the rough and irregular small pitches on the smooth surface with the stacking of the two-dimensional
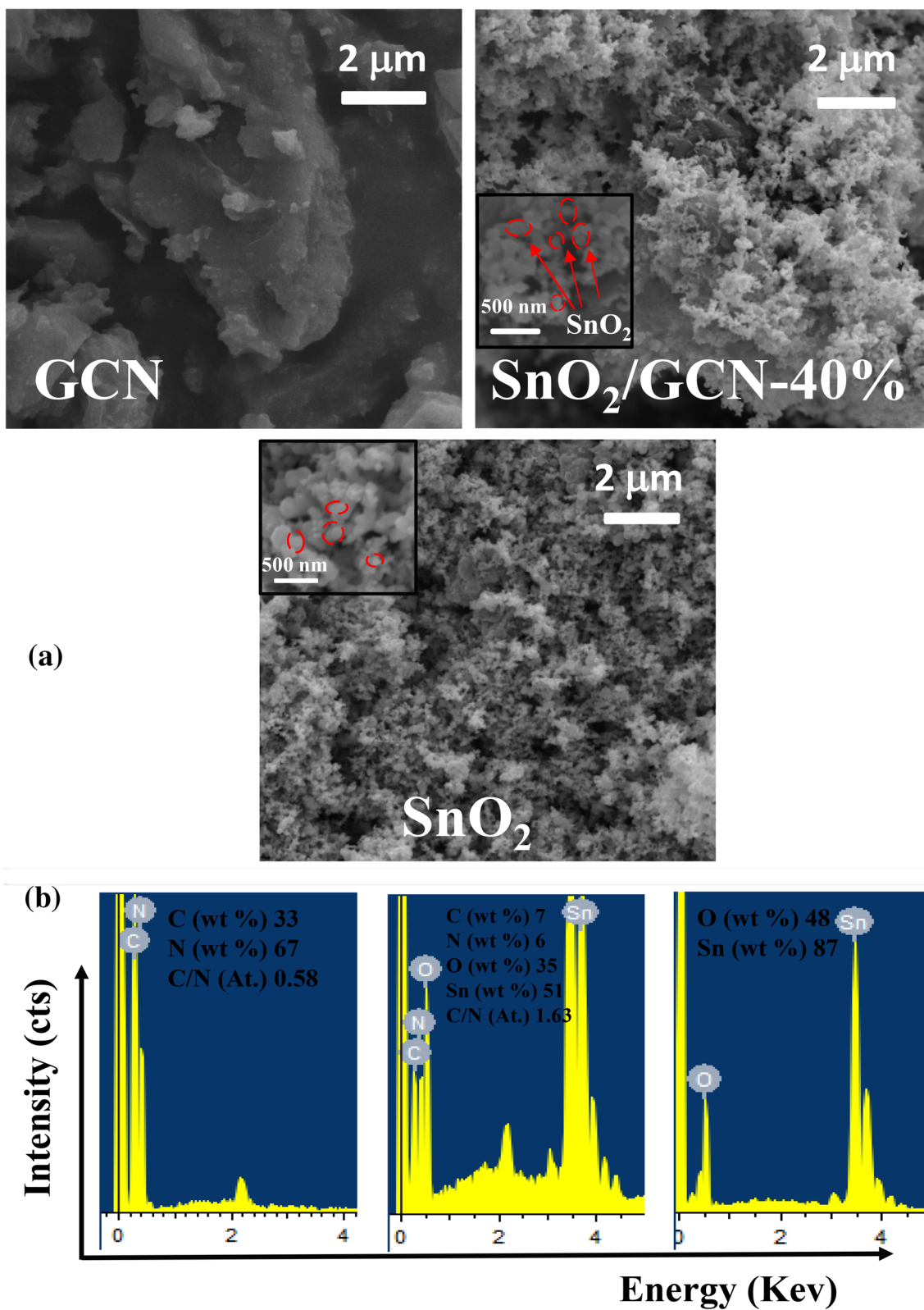
Fig. 1 SEM (**a**) and EDX (**b**) analysis of GCN, SnO$_2$, and coral-shaped SnO$_2$/GCN-40%

layers of the NSs. The SEM images of the pure SnO_2 showed the agglomeration of irregular-shaped SnO_2 NPs and the agglomeration of NPs was increased at the nanoscale. The approximate size of the pure SnO_2 NPs was found as 20–40 nm, as shown in the red circles in the SEM images of SnO_2. The SEM images of SnO_2/GCN nanocomposite showed the formation of the coral-like structure after the incorporation of SnO_2 NPs on GCN nanosheets. Due to the electrostatic forces in GCN and π bonding, the nanoparticles of SnO_2 were bridged together with GCN nanosheets and formed a tree kind of structure that resembles more like a coral in the sea. This is adventitious as during the formation of the interlinked structure between SnO_2 and GCN, there is more chances of morphological and electronic band modifications of GCN [37].

Surface chemical analysis of samples through EDX was used to identify the formation of SnO_2/g-C_3N_4 nanocomposite and the EDX spectrum of the samples is displayed in Fig. 1b. Elemental peaks of C, N, Sn, and O at their respective energy values in the spectrum showed their presence in the samples. No impurity peak was found in the EDX spectrum of GCN, SnO_2/GCN-40%, and SnO_2. The Sn peak in EDX spectrum of SnO_2/GCN-40% nanocomposite showed the successful incorporation of SnO_2 with the GCN by a proper preparation process. Table 1 shows the comparison of elemental percentages in the as prepared samples.

It can be seen from Table 1 that the C/N atomic ratio of GCN (0.58) was less than the predicted C/N value of g-C_3N_4 (0.75), whereas it was higher for SnO_2/GCN-40% (1.63). The small C/N ratio of GCN as compared to theoretical predicated C/N ratio, was assigned to incomplete condensation, but a higher C/N of SnO_2/GCN-40% nanocomposites was assigned to structural defects and high charge transport property [38].

XRD patterns of GCN, SnO_2 power, and SnO_2/GCN-40% are displayed in Fig. 2a. XRD analysis of GCN showed the two peaks. The first peak was observed at two-theta (2θ) of 27.53°, and the second peak was present at 2θ of 12.80°. The first peak was indexed to (002) plane of the graphitic structure. It reflected the interlayer stacking of the conjugated heptazine of tris-s triazine aromatic structure. The second peak was indexed (001) plane and assigned to the intra-planar tri-s-triazine periodic structure in the packing. Both

GCN (001, 002) peaks were indexed to the hexagonal phase of g-C_3N_4 (JCPDS-01–087-1526). XRD patterns of pure SnO_2 powder showed the diffraction peaks at 2θ of 26.7°, 34.11°, 38.3°, 52.2°, 62.3°, and 79.0°, which were indexed to (110), (101), (200), (211), (310) and (321) diffraction planes for SnO_2 crystalline structure (JCPDS-00-001-0657). In the case of SnO_2/GCN-40% heterojunction, XRD patterns showed a small shift and change in appearance of the main peak as compared to main peaks of GCN and SnO_2. The peak at 26.59° in SnO_2/GCN-40% was broader than GCN (27.53°, 002) peak, but narrow than SnO_2 (26.7°, 110) peak. This small shift and variation in peak appearance of SnO_2/GCN-40% can be assigned to close physical contact between combing nanomaterials and SnO_2 electronic coordination with the nitrogen of GCN. The intercalation of SnO_2 in the regular stacking of GCN could create structural defects and enlarge the inter-planar separation of tri-s-triazine packing by exfoliation of smaller parts to basic sheets [39].

To further study nanocomposites formation, the FTIR spectra of GCN, SnO_2, and SnO_2/GCN were obtained and displayed in Fig. 2b. GCN spectrum showed several peaks at (1226, 1313, 1395, 1540, and 1620 cm^{-1}) between 1200 and 1700 cm^{-1}, which were assigned to the stretching of C–N heterocyclic or typical C–N, and C=N stretching vibration modes. GCN peak at 804 cm^{-1} was attributed to the characteristics vibrations of the s-triazine ring units. FTIR patterns of GCN obtained on absorption profiles of SnO_2/GCN, which showed the shifts in (1239, 1402, 1635 cm^{-1}) peaks. These peak-shifts were assigned to the coordination between Sn and N atoms of melon units. The intensity of the broad peak (2620–3520 cm^{-1}) of SnO_2/GCN-40% was decreased as compared to GCN because of SnO_2 loading. The decrease in intensity of the broad peak of SnO_2/GCN-40% can be attributed to the structural defects and decrease in free uncondensed amino bonds on the surface of the nanocomposite. Overall, the absorption peaks intensities of SnO_2/GCN-40% nanocomposite was less than GCN. This decrease in GCN absorption intensities in nanocomposite was assigned to a unique structure in SnO_2/GCN-40%. Furthermore, the hydrophilic nature of GCN could also enhance the dispersion of metallic oxide NPs onto GCN.

It can be seen in UV–Vis DRS spectra from Fig. 2c that the absorption of visible light (400 nm) was increased with increasing content of SnO_2 in the nanocomposites. Nanocomposite containing 40% of SnO_2 has shown the highest absorption of the light than that of the other prepared samples. Band-gap energy of GCN, SnO_2, and SnO_2/GCN-40% were calculated as 3.70, 2.67, and 2.60 eV using the absorption edge values of 335, 464, and 475 nm with the help of formula (1240/Absorption Edge). Both narrow bandgap and the higher visible light absorption of SnO_2/GCN-40% showed the creation of defect levels at the bottom of the conduction band. These factors were crucial and could be

Table 1 Comparison of GCN, SnO_2/GCN-40%, and SnO_2 EDX elemental analysis

Samples	Wt. % Sn	Wt. % O	Wt. % C	Wt. % N	C/N ratio (atomic)
GCN	–	–	33	67	0.58
SnO_2/GCN-40%	51	35	7	6	1.63
SnO_2	87	48	–	–	–

Fig. 2 XRD (**a**), FTIR (**b**), UV–Vis DRS (**c**), Raman (**d**), PLS (**e**), and particle size distribution curve (**f**) of GCN, SnO$_2$/GCN-40%, and SnO$_2$. PLS was recorded under an excitation wavelength of 457 nm
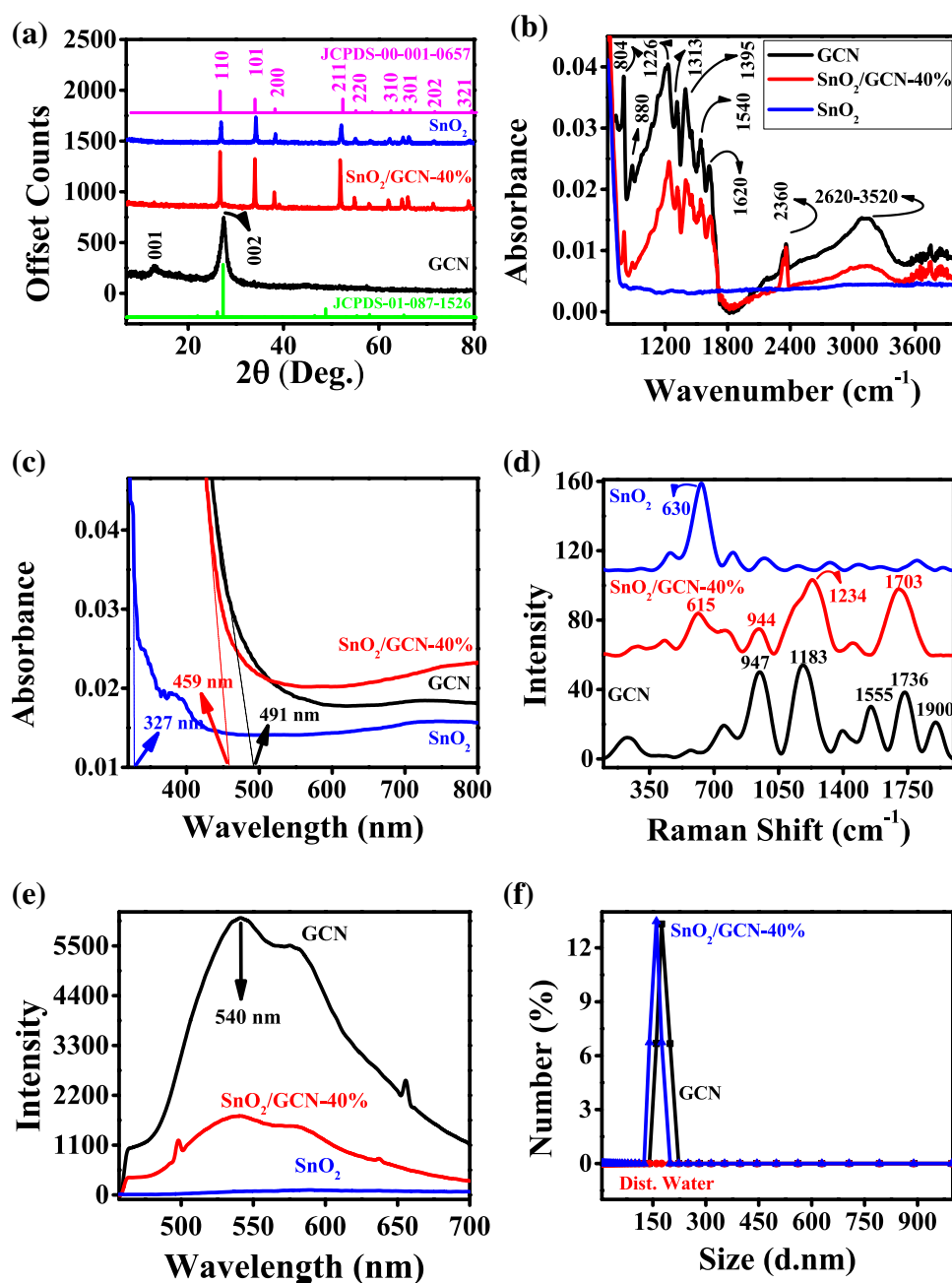
considered as one of the main reasons for the highest charge separation and electron-transferability of an efficient SnO$_2$/GCN-40% catalyst during the colorimetric sensor applications [40].

The graphitic and SnO$_2$ interaction in the nanocomposites was found by the analysis of Raman spectra. The Raman spectra of prepared samples are shown in Fig. 2d. GCN has displayed characteristics peaks at 947 cm^{-1}, 1183 cm^{-1} (D-band), and 1555 cm^{-1}, 1736 cm^{-1}, 1900 cm^{-1} (G-band). Graphitic band (G-band) was originated from the typical graphitic structure, and defect band (D-band) was originated from the defects present on the disordered carbon.

Pure SnO$_2$ has shown the main-peak at 630 cm^{-1}. All the characteristics Raman peaks of GCN and SnO$_2$ were present in SnO$_2$/GCN-40% nanocomposite spectra. SnO$_2$ and GCN interaction decreased the intensity of the main-peak of SnO$_2$, and the peak position was shifted downward for 15 cm^{-1}. The D-band was broadened, and the intensity ratio of D-band (1234 cm^{-1}) to the G-band (1703 cm^{-1}) band was calculated as 1.061 for SnO$_2$/GCN-40% nanocomposite. These factors showed higher structural defects in the SnO$_2$/GCN-40% nanocomposite as compared to the ordered graphitic structure in GCN. This structural-defect in SnO$_2$/GCN-40% could enhance its peroxidase-like activity [41].

PL emission spectra of GCN, SnO$_2$/GCN-40%, and SnO$_2$ are displayed in Fig. 2e. The electron transfer and separation behavior of GCN and SnO$_2$/GCN-40% were investigated by comparing corresponding PL emission intensities at 540 nm. PL emission is related to separation and electron transfer rate. The PL intensity of SnO$_2$/GCN-40% nanocomposite was lower than that of GCN because of the higher photo-generated electron–hole pair's separation efficiency. This decrease in PL intensity of SnO$_2$/GCN-40% was attributed to the heterojunction formation between both coupling semiconductors.

The particle size distribution in the suspension of the samples is measured by using the DLS analysis, and the number of particles versus the size graph is displayed in Fig. 2f. The mean hydrated diameter for the GCN and SnO$_2$/GCN-40% NSs were calculated as 175 and 160 nm respectively. The large size of GCN NSs as compared to SnO$_2$/GCN-40% NSs showed that the anchoring of SnO$_2$ with GCN has little or no influence on the crystallite size of the phase structure of SnO$_2$ NPs. Furthermore, the DLS analysis showed that the prepared SnO$_2$/GCN-40% NSs were monodispersed in the water solution and remained stable without any aggregation.

## Peroxidase activity of the nanocomposites

Colorimetric method

The catalytic activity of the prepared samples was figured out using a colorimetric bioassay. In this assay, chromogenic dye (TMB) was oxidized under the catalytic effect of NSs and oxidants, which turned the reaction mixture to blue. The naked eye could assess this blue color, and the UV–Vis absorption spectrum showed a peak at 654 nm of this blue color. It can be seen from curve (a–d) in Fig. 3a that no redox reaction occurred and no blue color (insert of the digital image in Fig. 3a) was developed for the reaction mixtures of SnO$_2$/GCN-40% suspension (a), SnO$_2$/GCN-40% and H$_2$O$_2$ (b), TMB and H$_2$O$_2$ (c), SnO$_2$/GCN-40% and TMB (d). In contrast, peroxidase reaction occurred, and the blue color was developed for the reaction mixtures of SnO$_2$/GCN-40%, TMB, and H$_2$O$_2$ with a prominent peak at 654 nm (e). The developed-blue color and absorbance value at 654 nm (A$_{654}$ nm) were related to a charge-transfer complex, which was formed by one-electron oxidation of TMB. The intensity of A$_{654}$ nm showed the high electron transferability and higher charge separation efficiency of the SnO$_2$/GCN-40% NSs. Therefore, the colorimetric approach showed that SnO$_2$/GCN-40% can act as a catalyst for the reaction between H$_2$O$_2$ and chromogenic dye [42].

Fluorometric quenching method

To further determine SnO$_2$/GCN-40% nanocomposite peroxidase-like catalytic nature, the fluorescence quenching approach was used. Chromogenic dye (RhB) was used as the fluorescence change agent during the reaction and for reaction signal readout. The SnO$_2$/GCN-40% nanocomposite can catalyze the reaction between RhB and H$_2$O$_2$. First, a prescan spectrum of the dye (70 ng mL^{-1}) was obtained using an excitation wavelength of 340 nm. The pre-scan spectrum showed that RhB exhibited maximum absorption and fluorescence emission peaks at 554–577 nm, respectively. Therefore, the fluorescence emission spectra of the different reaction mixtures were scanned between 550 and 800 nm under an excitation of 554 nm, and the resultant curves are

(a)

(b)
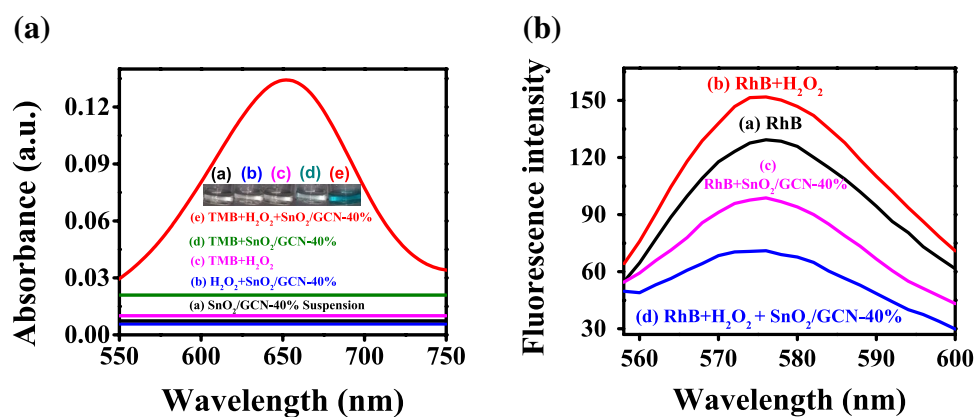
Fig. 3 UV–Vis absorption spectrum of the reaction mixtures containing SnO$_2$/GCN-40% (a) H$_2$O$_2$ + SnO$_2$/GCN-40% (b), TMB + H$_2$O$_2$ (c), TMB + SnO$_2$/GCN-40% (d), and TMB + H$_2$O$_2$ + SnO$_2$/GCN-40% (e) with corresponding digital images in the insert (**a**). Fluorescence spectrum of RhB (a), RhB + H$_2$O$_2$ (b), RhB + SnO$_2$/GCN-40% (c) and RhB + SnO$_2$/GCN-40% + H$_2$O$_2$ (d) reaction mixtures

(**b**). Reaction conditions were [SnO$_2$/GCN-40%] = 15.58 μg mL^{-1}, pH = 5.0, reaction time = 30 s, reaction temperature = room temperature, [RhB] = 70 ng mL^{-1}, [TMB] = 300 μM, colorimetric analysis buffer = 0.1 M sodium acetate, fluorescence analysis buffer = 0.1 M PBS, and [H$_2$O$_2$] of 655 μM

labelled as curve (a–d) in Fig. 3b. A comparison of peak intensities at 577 nm showed that RhB fluorescence intensity (a) was enhanced in the presence of H_2O_2 (b). This enhanced fluorescence intensity of RhB and H_2O_2 reaction mixture can be attributed to the chromophoric effect added by H_2O_2 in the reaction mixture [5]. The addition of SnO$_2$/GCN-40% suspension in the RhB solution has resulted in a decrease in fluorescence intensity as shown in curve (c). This decrease in fluorescence intensity was assigned to the adsorption of RhB dye on the surface of SnO$_2$/GCN-40% NSs. However, the fluorescence intensity of the reaction mixture containing RhB and SnO$_2$/GCN-40% NSs was further reduced upon the addition of H_2O_2 as shown in curve (d) because of the oxidation of RhB by H_2O_2 in the presence of SnO$_2$/GCN-40% NSs as a catalyst. SnO$_2$/GCN-40% NSs acted as a catalyst and split H_2O_2 into radicals like hydroxyl radicals and ions, which could oxidize RhB. As a result of RhB oxidation, the fluorescence intensity of the reaction mixture of RhB, SnO$_2$/GCN-40%, and H_2O_2 was decreased. Therefore, fluorescence experimental results showed that SnO$_2$/GCN-40% acted as a peroxidase-like catalyst for the reaction between chromogenic dye and H_2O_2 [5, 43].

Optimization of the reaction conditions for colorimetric sensor

The acceptance, transfer, and donation of electrons through graphitic structure affected the peroxidase-like activity of the catalyst in a redox reaction [44]. Therefore, for designing good performance sensor, variables such as the amount of the metal oxide, temperature, time, pH of the buffer, NSs amount, and TMB concentrations, were required to optimize. A_{654} nm represented the catalytic peroxidase-like activity of NSs; therefore, the above reaction conditions were adjusted by finding their effect on the A_{654} nm at a constant $[H_2O_2]$ as 655 μM, as shown in Fig. 4.

The catalytic activity of SnO$_2$/GCN nanocomposites was depended upon the amount of metal oxide. The effect of prepared-samples oxidation power on the A_{654} nm was determined and displayed in Fig. 4a. The A_{654} nm of the reaction mixture containing NSs of coral-shaped SnO$_2$/GCN-40% was higher than A_{654} nm of the rest of the prepared nanomaterials. So, the peroxidase-like catalytic activity of SnO$_2$/GCN-40% was higher than the peroxidase-like activity of GCN, SnO$_2$/GCN-20%, SnO$_2$/GCN-60%, SnO$_2$/GCN-80%, and pure SnO$_2$ NPs. The synergistic effect between SnO$_2$ on the thin NSs of GCN has imparted a role in enhancing the peroxidase-like catalytic activity of coral-shaped SnO$_2$/GCN-40%. These experimental results were matched with the novel functionalities in SnO$_2$/GCN-40% like nanostructuring, optical and electronic properties of the least rate of electron–hole pair's recombination and high electron conductivity. The higher peroxidase-like activity of SnO$_2$/

GCN-40% nanocomposites showed that SnO$_2$/GCN-40% can provide additional active sites for the reaction between TMB and H_2O_2 as compared to other samples. As a result, more light-targeted radical reactive species and ions were produced from the H_2O_2 under the catalytic influence of SnO$_2$/GCN-40% to oxidize TMB.

The effect of reaction temperature and reaction time is shown in Fig. 4b and c. It can be seen in Fig. 4b that the prepared sensor does not give a uniform response with the reaction time. Initially, A_{654} nm was increased, reached a maximum value at 30 s of the reaction time. Finally, it started to decrease as the reaction time was further prolonged. It can be seen from Fig. 4c that A_{654} nm is increased as the reaction temperature is raised. The changes in A_{654} nm with the temperature can be explained in terms of the collision frequency and the electron transferability behavior of the nanozymes. With a rise in reaction temperature, the collision frequency was increased and the number of the collision taking part in the reaction were also increased. Furthermore, the electron-transferability of the prepared semiconductor nanomaterials was also increased with an increase in temperature. However, for the convenience of the reaction conditions, the rest of the measurements were performed at room temperature. Therefore, it was better to measure the A_{654} nm of the reaction mixture within 30 s of the reaction time and at room temperature.

The response of colorimetric sensors was not stable with variable pH. Reactions of TMB with H_2O_2 under the catalytic effect of SnO$_2$/GCN-40% were studied in acidic, neutral, and basic conditions, and the resultant graph of A_{654} nm versus various pH is displayed in Fig. 4d. The maximum A_{654} nm for the reaction mixture of TMB, H_2O_2, and SnO$_2$/GCN-40% NSs was observed at pH 5.0. This maximum value of A_{654} nm was assigned to the good and stable peroxidase-like catalytic activity of SnO$_2$/GCN-40% NSs at pH 5.0, which was chosen as the optimum pH conditions for the subsequent study of SnO$_2$/GCN-40% catalytic activity. The peroxidase-like activity of SnO$_2$/GCN-40% NSs was much higher in weakly-acidic buffer solution than in basic and neutral buffer solutions. The optimum value of pH in the weakly acidic range showed that TMB was easily oxidized because of an increase in the number of reacting NSs, and by a decrease in deviations for blue-colored reaction mixture. This effect of pH on the peroxidase-like activity of the SnO$_2$/GCN-40% catalyst was the same as stated for some nanomaterials-based peroxidase-mimetics and horseradish peroxide (HRP) [45–47].

The effect of the amount of SnO$_2$/GCN-40% NSs ([SnO$_2$/GCN-40%]) on A_{654} nm is shown in Fig. 4e. The increase in A_{654} nm with [SnO$_2$/GCN-40%] was attributed to the peroxidase-like activity of the NSs. A linear relationship between the A_{654} nm versus [SnO$_2$/GCN-40%] from 10 to 300 μg mL^{-1} was obtained, as shown in the insert image of

Fig. 4 Influence of percentage of SnO$_2$ (**a**), reaction temperature (**b**), the response time (**c**), pH of buffer (**d**), amount of SnO$_2$/GCN-40% (**e**), and concentration of TMB (**f**) on the colorimetric response of the sensor. All reaction conditions were the same, as mentioned in Fig. 3
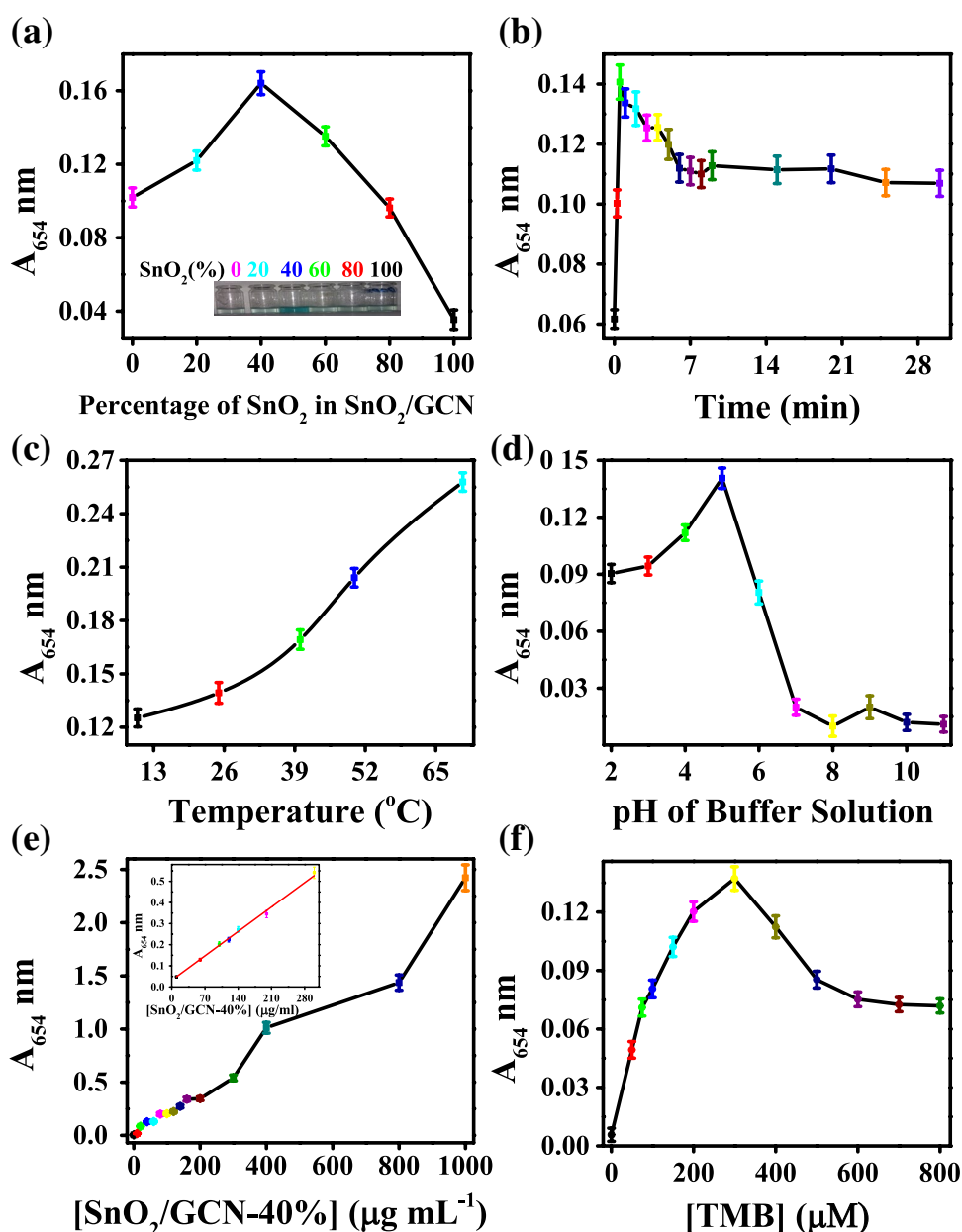

Fig. 4e. But, during the experimentation, the 15.58 µg mL^{-1} of [SnO$_2$/GCN-40%] was chosen as a suitable amount for sensor development. The concentration of TMB ([TMB]) also affected the performance of the detection system. Therefore, a plot of A$_{654}$ nm versus various [TMB] was obtained to find the suitable amount for the chromogenic agent, and the resultant graph is displayed in Fig. 4f. Experimental results showed that the variable [TMB] has a significant effect on the reaction between H$_2$O$_2$ and TMB because of peroxidase-like SnO$_2$/GCN-40% NSs. The A$_{654}$ nm of the reaction system was increased with the rise in [TMB] from 0 to 300 µM at first. Further increase in [TMB] beyond 300 µM has shown a decrease in A$_{654}$ nm because of the reduction of the catalytic activity of SnO$_2$/GCN-40% NSs. The

maximum reaction performance was obtained at 300 µM of [TMB], because at this stage, the reaction reached a saturation point and the SnO$_2$/GCN-40% NSs showed the highest peroxidase-like activity at this concentration of TMB. Thus, 300 µM of [TMB] was considered as the optimum amount for best sensor performance, and this [TMB] was used in further analysis.

Mechanism of the developed sensor

The catalytic mechanism of the sensor was studied by using steady-state kinetics of the reaction [48]. Initial velocity for both H$_2$O$_2$ and TMB were found from the slopes of linear portion of A$_{654}$ nm versus time curves.

Then, Beer-Lambert law [$A = \varepsilon Cl$, where A was absorbance, ε was extinction coefficient ($\varepsilon = 39{,}000$ M^{-1} cm^{-1}), C is concentration of substrate, 'l' was path length (l = 1 cm)] was applied for the determination of concentration of oxidized TMB. Steady-state kinetics of the reactions with substrates (H$_2$O$_2$ or TMB) was determined by varying the concentration of one substrate and taking other conditions constant. Typical Michaelis–Menten curves were obtained for both H$_2$O$_2$ and TMB, as shown in Fig. 5a and b. Double reciprocal plots were obtained by using initial reaction rates. In Fig. 5c, a straight line plot between reciprocal of initial velocity against reciprocal of H$_2$O$_2$ concentration was obtained at constant TMB concentration (300 µM). Similarly, a straight line plot between reciprocal of initial velocity against reciprocal of TMB concentrations was obtained at constant H$_2$O$_2$ concentration (655 µM), as shown in Fig. 5d. The double reciprocal plot at different concentrations of TMB (300,

250, and 200 µM) for reciprocal of initial velocity against various reciprocal of H$_2$O$_2$ concentrations is shown in Fig. 5e. Similarly, a double reciprocal plot at different concentrations of H$_2$O$_2$ (655, 550, and 450 µM) for reciprocal of initial velocity against reciprocal of TMB concentrations is shown in Fig. 5f. Three approximate parallel lines were obtained in the double reciprocal plots, which showed that the slopes of the double reciprocal plots are almost parallel. The parallel slops in the double reciprocal plots were the characteristics of a ping-pong mechanism. Furthermore, the maximal reaction velocity (V_{max}) and Michaelis–Menten constant (K_m) were calculated from the Line weaver-Burk plot. The calculated V_{max} and K_m values are shown in Table 2. The K_m values represent the affinity for the substrate. The smaller K_m showed a higher affinity between nanomaterial and the substrate. The K_m value for SnO$_2$/GCN-40% (0.002 mM) was lower than that of HRP (2.75 mM) when the TMB

Fig. 5 Catalytic mechanism and a steady-state kinetic assay of SnO$_2$/GCN-40%. The concentration of TMB was 300 µM and H$_2$O$_2$ concentration was varied. (**a**) The concentration of H$_2$O$_2$ was 655 µM and TMB concentration was varied. (**b**) Double reciprocal plots of catalytic activity of SnO$_2$/GCN-40% with the concentration of one substrate was fixed (TMB or H$_2$O$_2$) and the other varied (**c** and **d**). Ping-Pong mechanism for H$_2$O$_2$ (**e**) and TMB (**f**). The initial velocity (V) of the reaction was determined using optimum reaction conditions, as mentioned in Fig. 3
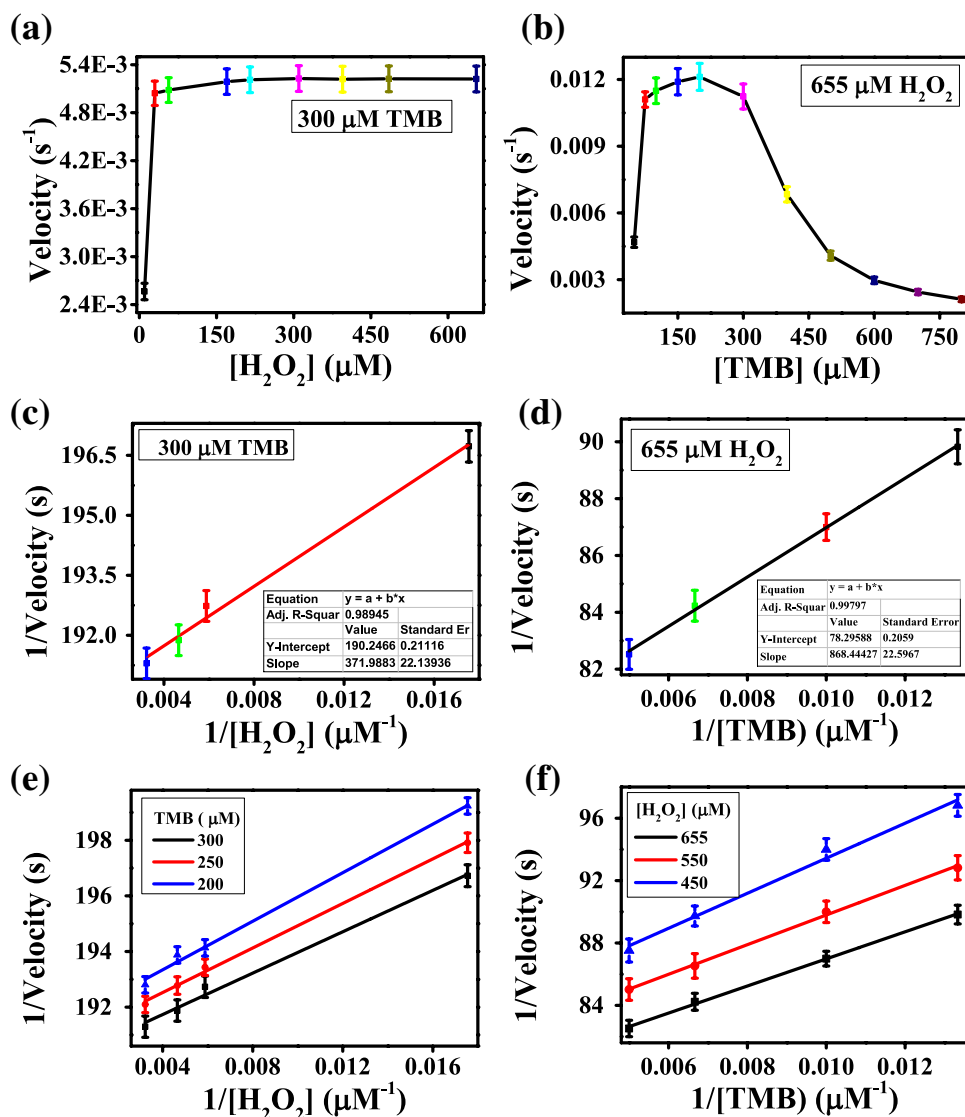
**Table 2** Maximum reaction rate (V_{max}) and Michaelis–Menten constant (K_m) of SnO$_2$/GCN-40% and HRP

Catalyst	Substrate	K_m (mM)	V_{max} (nM s^{-1})	References
HRP enzyme	TMB	0.275	12.4	[49]
	H$_2$O$_2$	0.214	24.6	
Coral-shaped SnO$_2$/GCN-40%	TMB	0.002	0.526	This work
	H$_2$O$_2$	0.01	1.28	

substrate was used. Similarly, the K_m value for SnO$_2$/GCN-40% (0.01 mM) was also lower than that of HRP (2.14 mM), when the H$_2$O$_2$ substrate was used. Therefore, these result indicated that SnO$_2$/GCN-40% have a high affinity with the substrate as compared to the natural enzyme of HRP [48].

Detection of H$_2$O$_2$

Based on the excellent peroxidase-like activity of SnO$_2$/GCN-40% NSs and novel properties, a colorimetric sensor for the determination of H$_2$O$_2$ by using TMB substrate at the optimum experimentation conditions was constructed. UV–Vis absorption curves at optimal reaction conditions (pH 5.0, 25 °C) with typical H$_2$O$_2$ concentrations ([H$_2$O$_2$]) of 10, 30, 57, 170, 215, 310, 395, 485, and 655 µM were obtained, as shown in Fig. 6a. The absorbance peak at 654 nm was increased as H$_2$O$_2$ was increased. For the dose–response curves, absorbance value at λ_{max} of 654 nm was plotted against various doses of [H$_2$O$_2$], and the resultant graphs are displayed in Fig. 6b. The A$_{654}$ nm versus [H$_2$O$_2$] plot did not stay linear for the whole range of H$_2$O$_2$ concentrations. The A$_{654}$ nm was increased as the

Fig. 6 UV–Vis absorption spectra of the sensor at 10, 30, 57, 170, 215, 310, 395, 485, and 655 µM of [H$_2$O$_2$] (**a**), corresponding A$_{654}$ nm versus [H$_2$O$_2$] plot in the range from zero to 7000 µM (**b**). Sensor linear calibration curve (**c**), recyclability of catalyst (**d**), and selectivity of sensor (**e**) for colorimetric H$_2$O$_2$ determination. All reaction conditions were the same, as mentioned in Fig. 3
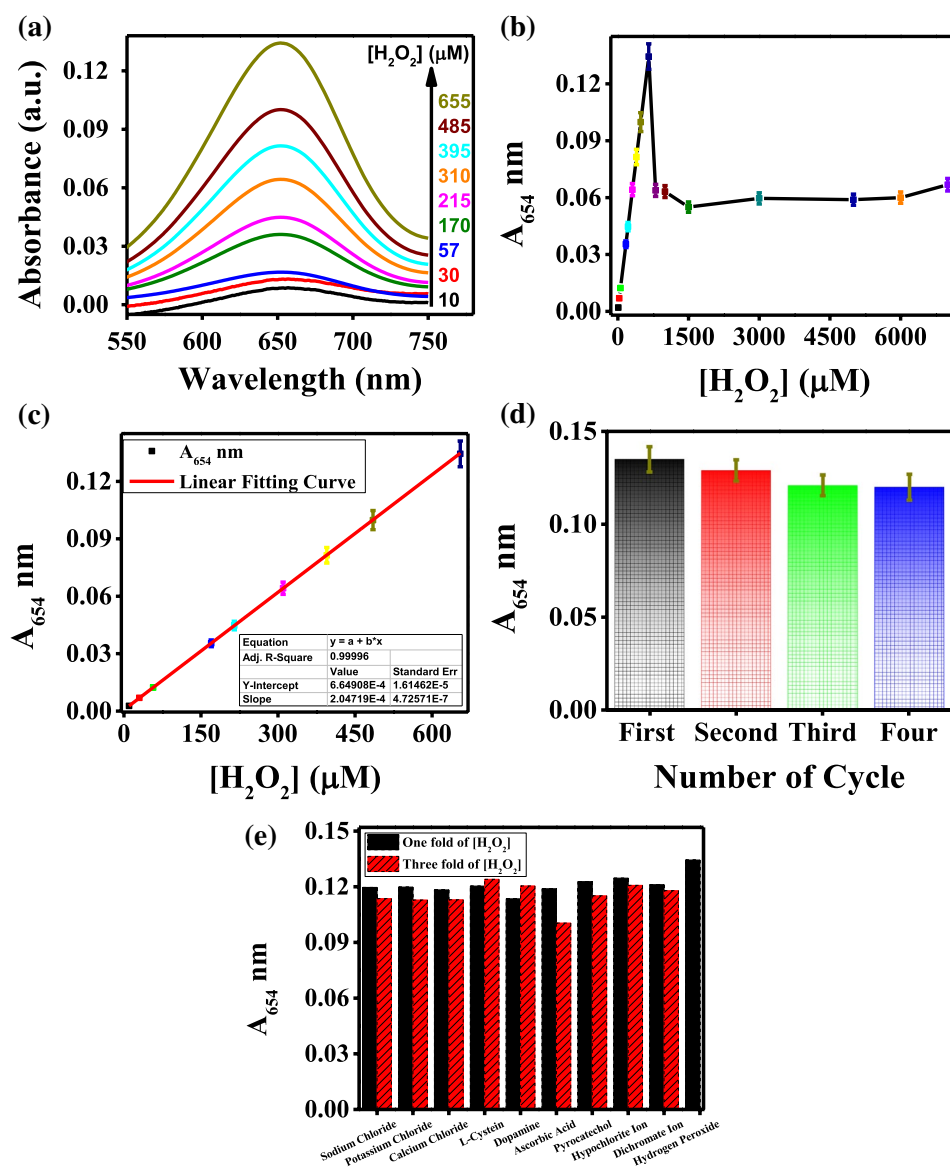
[H₂O₂] was increased (10 − 655 μM), reached the maximum value for 655 μM of [H₂O₂]. At this stage, the reaction was reached a saturation point about the dose of the sensor. Further addition of H₂O₂ at this equilibrium point, has hindered the catalytic activity of SnO₂/GCN-40% NSs, and A₆₅₄ nm was decreased. The linear range and linear regression equation were determined from the calibration curve to simplify the sensing procedure. The calibration curve of the developed sensor is presented in Fig. 6c, which showed that the developed sensor exhibited a linear response from 10 to 655 μM of [H₂O₂] with a linear regression equation $\left(A_{654} = 2.05 \times 10^{-4}[H_2O_2] + 6.65 \times 10^{-4}\right)$ and correlation coefficient (R^2) of 0.99996.

Limit of detection ($\frac{3.3\sigma}{s}$) and the limit of quantification $\left(\frac{10\sigma}{s}\right)$ were calculated using standard-error of estimate (σ) and the slope of linear-regression-line (s) to find the validity of the designed sensor. The LOD and LOQ were determined as 0.3 and 0.8 μM, respectively. LOD and linear range of this sensor was compared with the already reported H₂O₂ sensors, and the comparison is presented in Table 3.

It can be seen from Table 3 that SnO₂/GCN-40% NSs based colorimetric sensor has higher peroxidase-like activity and superior properties than some other reported sensors. This work has a lower limit of detection as compared to the LODs of sensors based on Ag NPs/SnO₂ Nanotubes, Hemin/SnO₂, SnO₂/Polyethylenimine/Graphene, Au/SnO₂ Micro tubes, SnO₂ Nanofibers, FePt-Au NPs, Fe₃O₄/Lignin NPs, MnSe/g-C₃N₄ NSs, V₂O₅ NPs, Reduced Co₃O₄ NPs, and

g-C₃N₄ Dots. Coral-shaped SnO₂/GCN-40% NSs based sensor have a broader linear range as compared to the linear ranges of Hemin/SnO₂, SnO₂ Nanofibers, Pd–Pt Nano cages/SnO₂/Graphene, SnO₂/α-Fe₂O₃/Prussian Blue, Hemin/SnO₂/Metglas, Prussian Blue Nano cubes/SnO₂/Reduced Graphene Oxide, HRP/Ni–SnO₂, Fe₃O₄/Lignin NPs, V₂O₅ NPs, Reduced Co₃O₄ NPs, g-C₃N₄ Dots, Fe₃O₄/g-C₃N₄ NSs and MoS₂ QDs/g-C₃N₄ based H₂O₂ sensors. Therefore, the current designed colorimetric sensor of coral-shaped SnO₂/GCN-40% has high sensitivity and simple in performance.

Recyclability and stability testing of SnO₂/GCN-40% peroxidase-like catalyst

The recyclability and stability of the coral-shaped SnO₂/GCN-40% nanocomposite was significant for the reaction of TMB with H₂O₂. To study the efficiency of SnO₂/GCN-40% after several recycle use, recycling tests at optimum reaction conditions was performed. Nanosheets of SnO₂/GCN-40% catalyst were recovered from the reaction mixture by centrifugation. Washed the SnO₂/GCN-40% NSs with sodium acetate buffer solution and later on dried in the oven for three hours at 80 °C before reusing them in subsequent cycling reactions. It can be seen from Fig. 6d that a small decrease in A₆₅₄ nm occurred even-after four reaction-cycles of the SnO₂/GCN-40% NSs. This small difference in A₆₅₄ nm was assigned to the loss of peroxidase-like catalyst during the recycling process. These experimental results showed that SnO₂/GCN-40% NSs remained stable during the recycling

Table 3 Comparison of linear ranges and LODs of the reported H₂O₂ sensors

Sample	Method	Linear range (μM)	LOD (μM)	References
Ag NPs/SnO₂ nanotubes	Electrochemical	10–35,000	5.0	[50]
Hemin/SnO₂	Electrochemical	1.5–90	1.5	[51]
SnO₂/Polyethylenimine/Graphene	Electrochemical	9–1640	1	[52]
Au/SnO₂ micro tubes	Electrochemical	10–1000	0.6	[53]
SnO₂ nanofibers	Electrochemical	2–160	0.5	[54]
Pd–Pt nano cages/SnO₂/graphene	Electrochemical	1–300	0.3	[55]
SnO₂/α-Fe₂O₃/Prussian blue	Electrochemical	20–332	0.27	[56]
Hemin/SnO₂/Metglas	Electrochemical	1–72	0.16	[57]
Prussian blue nano cubes/SnO₂/ reduced graphene oxide	Electrochemical	25–225	0.071	[58]
HRP/Ni–SnO₂	Electrochemical	0.1–300	0.043	[59]
FePt-Au NPs	Colorimetric	20–700	12.33	[60]
Fe₃O₄/lignin NPs	Colorimetric	5–100	2	[61]
MnSe/g-C₃N₄ NSs	Colorimetric	18–1800	1.8	[62]
V₂O₅ NPs	Colorimetric	1–500	1	[63]
Reduced Co₃O₄ NPs	Colorimetric	1–30	0.43	[64]
g-C₃N₄ dots	Colorimetric	1–100	0.4	[65]
Fe₃O₄/g-C₃N₄ NSs	Colorimetric	1–40	0.3	[66]
MoS₂ QDs/g-C₃N₄	Colorimetric	2–50	0.02	[67]
Coral-shaped SnO₂/GCN NSs	Colorimetric	10–655	0.3	Present work

process without any destruction sign and loss of peroxidase-like activity.

Selectivity of sensor

Apart from sensitivity and repeatability analysis, selectivity testing is very important to determine the performance of a sensor. To find the selectivity of the proposed sensing system, the absorbance responses of the proposed sensor were investigated for several potential interfering and coexisting substances. The absorption signals were recorded in the presence of interfering species in the reaction mixture of SnO_2/GCN-40%, TMB, and H_2O_2 at the optimum reaction conditions. The concentration of interfering species was taken as one fold (655 μM) and three-fold of H_2O_2 concentration. As shown in Fig. 6e, a higher absorption at 654 nm was measured only if H_2O_2 was present in the reaction mixture of SnO_2/GCN-40% and TMB. On the contrary, no significant change of absorption signal was found by adding other interfering substances such as sodium chloride, potassium chloride, calcium chloride, L-cysteine, dopamine, ascorbic acid, uric acid, pyrocatechol, dichromate ions, and hypochlorite ions in the reaction mixture of SnO_2/GCN-40%NSs, H_2O_2, and TMB. Therefore, these control samples did not affect the determination of H_2O_2. These results also demonstrated that the SnO_2/GCN-40% based colorimetric assay can discriminate H_2O_2 from other coexisting species. Therefore, the developed SnO_2/GCN-40% based colorimetric sensor was specific for H_2O_2 detection and can be applied for H_2O_2 determination in the presence of other oxidants. The high selectivity of the sensor for H_2O_2 sensing can be assigned to the strong binding-affinity between coral-shaped SnO_2/GCN-40% NSs and H_2O_2 [48].

Conclusion

In summary, a new colorimetric sensor for sensitive determination of H_2O_2 was developed based on improving the structural, optical, and electrical properties of GCN by SnO_2 nanoparticles. The formation and improved properties of prepared samples were confirmed through microscopy and spectroscopy techniques. The coral-shaped SnO_2/GCN-40% has shown the optimal loading of SnO_2 nanoparticles, structural defects, low rate of charge carriers' recombination, and high electron-transferability. The reaction mixture containing 15.58 μg mL^{-1} of SnO_2/GCN-40% nanosheets, 300 μM of TMB, and 655 μM of H_2O_2 has shown the maximum blue color and absorbance at 654 nm as compared to the rest of the prepared samples if the pH of the buffer was 5.0 and the reaction measurements were done after 30 s at room temperature. So, the colorimetric H_2O_2 sensor was designed using the nanosheets of coral-shaped SnO_2/GCN-40%. A

linear range of 10–655 μM was obtained from the calibration plot with a correlation coefficient of 0.99996 at the sensor optimal conditions. The H_2O_2 detection limit of the sensor was 0.3 μM. The designed-colorimetric sensor has advantages of simplicity, ease of production, low cost, sensitivity, and selective. This colorimetric sensor gave a fast and rapid response within thirty seconds for H_2O_2 detection. Furthermore, the colorimetric sensor of coral-shaped SnO_2/GCN-40% followed the Michaelis–Menten equation and showed a higher affinity toward reaction substrates as compared to horseradish peroxide. The good catalytic activity of the prepared SnO_2/GCN-40% nanocomposite can create a potential for developing faster, safer, convenient, and real-time sensor devices for application in food safety, clinical diagnosis, environmental monitoring, and industrial processing in near future. This work will likely inspire future engineering of nanozyme materials, which can enable applications of nanostructured materials in analytical chemistry and nanomedicine field.

Compliance with ethical standards

Conflict of interest The authors declare no competing financial interest.

References

1. Teodoro, K.B.R., Migliorini, F.L., Christinelli, W.A., Correa, D.S.: Detection of hydrogen peroxide (H_2O_2) using a colorimetric sensor based on cellulose nanowhiskers and silver nanoparticles. Carbohydr. Polym. **212**, 235–241 (2019)

2. Pang, S., Zhang, Y., Wu, C., Feng, S.: Fluorescent carbon dots sensor for highly sensitive detection of guanine. Sens. Actuators B Chem. **222**, 857–863 (2016)

3. Hong, J., Maguhn, J., Freitag, D., Kettrup, A.: Determination of H_2O_2 and organic peroxides by high-performance liquid chromatography with post-column UV irradiation, derivatization and fluorescence detection. Fresenius J. Anal. Chem. **361**(2), 124–128 (1998)

4. Klassen, N.V., Marchington, D., McGowan, H.C.E.: H_2O_2 Determination by the I_3^- method and by $KMnO_4$ titration. J. Anal. Chem. **66**(18), 2921–2925 (2002)

5. Siddiqui, A.S., Ahmad, M.A., Nawaz, M.H., Hayat, A., Nasir, M.: Nitrogen-doped graphene oxide as a catalyst for the oxidation of Rhodamine B by hydrogen peroxide: application to a sensitive fluorometric assay for hydrogen peroxide. Microchim. Acta **187**(1), 47 (2019)

6. Pratsinis, A., Kelesidis, G.A., Zuercher, S., Krumeich, F., Bolisetty, S., Mezzenga, R., Leroux, J.C., Sotiriou, G.A.: Enzyme-mimetic antioxidant luminescent nanoparticles for highly sensitive hydrogen peroxide biosensing. ACS Nano **11**(12), 12210–12218 (2017)

7. Haddad Irani-Nezhad, M., Hassanzadeh, J., Khataee, A., Orooji, Y.: A chemiluminescent method for the detection of H_2O_2 and glucose based on intrinsic peroxidase-like activity of WS_2 quantum dots. Molecules **24**(4), 689 (2019)

8. Lin, J.-R., Chu, C.-J., Venkatesan, P., Wu, S.P.: Zinc (II) and pyrophosphate selective fluorescence probe and its application to living cell imaging. Sens. Actuators B Chem. **207**, 563–570 (2015)

9. Wang, T., Zhu, H., Zhuo, J., Zhu, Z., Papakonstantinou, P., Lubarsky, G., Lin, J., Li, M.: Biosensor based on ultrasmall MoS_2 nanoparticles for electrochemical detection of H_2O_2 released by cells at the nanomolar level. Anal. Chem. **85**(21), 10289–10295 (2013)

10. Tao, Y., Ju, E., Ren, J., Qu, X.: Bifunctionalized mesoporous silica-supported gold nanoparticles: intrinsic oxidase and peroxidase catalytic activities for antibacterial applications. Adv. Mater. **27**(6), 1097–1104 (2015)

11. Nasir, M., Nawaz, M.H., Latif, U., Yaqub, M., Hayat, A., Rahim, A.: An overview on enzyme-mimicking nanomaterials for use in electrochemical and optical assays. Microchim. Acta **184**(2), 323–342 (2016)

12. Nasir, M., Rauf, S., Muhammad, N., Hasnain Nawaz, M., Anwar Chaudhry, A., Hamza Malik, M., Ahmad Shahid, S., Hayat, A.: Biomimetic nitrogen doped titania nanoparticles as a colorimetric platform for hydrogen peroxide detection. J. Colloid Interface Sci. **505**, 1147–1157 (2017)

13. Liu, J., Wang, H., Antonietti, M.: Graphitic carbon nitride "reloaded": emerging applications beyond (photo) catalysis. Chem. Soc. Rev. **45**(8), 2308–2326 (2016)

14. Li, X.H., Chen, J.S., Wang, X., Sun, J., Antonietti, M.: Metal-free activation of dioxygen by graphene/g-C_3N_4 nanocomposites: functional dyads for selective oxidation of saturated hydrocarbons. J. Am. Chem. Soc. **133**(21), 8074–8077 (2011)

15. Ge, L., Han, C., Liu, J., Li, Y.: Enhanced visible light photocatalytic activity of novel polymeric g-C_3N_4 loaded with Ag nanoparticles. Appl. Catal. A Gen. **409–410**, 215–222 (2011)

16. Fu, J., Yu, J., Jiang, C., Cheng, B.: g-C_3N_4-Based heterostructured photocatalysts. Adv. Energy Mater. **8**(3), 1701503 (2018)

17. Patnaik, S., Martha, S., Parida, K.M.: An overview of the structural, textural and morphological modulations of g-C_3N_4 towards photocatalytic hydrogen production. RSC Adv. **6**(52), 46929–46951 (2016)

18. Ren, H., Yan, L., Liu, M., Wang, Y., Liu, X., Liu, C., Liu, K., Zeng, L., Liu, A.: Green tide biomass templated synthesis of molybdenum oxide nanorods supported on carbon as efficient nanozyme for sensitive glucose colorimetric assay. Sens. Actuators B Chem. **296**, 126517 (2019)

19. Ren, H., Liu, X., Yan, L., Cai, Y., Liu, C., Zeng, L., Liu, A.: Ocean green tide derived hierarchical porous carbon with bi-enzyme mimic activities and their application for sensitive colorimetric and fluorescent biosensing. Sens. Actuators B Chem. **312**, 127979 (2020)

20. Yan, L., Ren, H., Guo, Y., Wang, G., Liu, C., Wang, Y., Liu, X., Zeng, L., Liu, A.: Rock salt type NiO assembled on ordered mesoporous carbon as peroxidase mimetic for colorimetric assay of gallic acid. Talanta **201**, 406–412 (2019)

21. Liu, X., Yan, L., Ren, H., Cai, Y., Liu, C., Zeng, L., Guo, J., Liu, A.: Facile synthesis of magnetic hierarchical flower-like Co_3O_4 spheres: Mechanism, excellent tetra-enzyme mimics and their colorimetric biosensing applications. Biosens. Bioelectron. **165**, 112342 (2020)

22. Han, L., Zeng, L., Wei, M., Li, C.M., Liu, A.: A V_2O_3-ordered mesoporous carbon composite with novel peroxidase-like activity towards the glucose colorimetric assay. Nanoscale **7**(27), 11678–11685 (2015)

23. Liu, P., Han, L., Wang, F., Li, X., Petrenko, V.A., Liu, A.: Sensitive colorimetric immunoassay of Vibrio parahaemolyticus based on specific nonapeptide probe screening from a phage display library conjugated with MnO_2 nanosheets with peroxidase-like activity. Nanoscale **10**(6), 2825–2833 (2018)

24. Han, L., Liu, P., Zhang, H., Li, F., Liu, A.: Phage capsid protein-directed MnO_2 nanosheets with peroxidase-like activity for spectrometric biosensing and evaluation of antioxidant behaviour. Chem. Commun. (Camb) **53**(37), 5216–5219 (2017)

25. Han, L., Shi, J., Liu, A.: Novel biotemplated MnO_2 1D nanozyme with controllable peroxidase-like activity and unique catalytic mechanism and its application for glucose sensing. Sens. Actuators B Chem. **252**, 919–926 (2017)

26. Liu, P., Wang, Y., Han, L., Cai, Y., Ren, H., Ma, T., Li, X., Petrenko, V.A., Liu, A.: Colorimetric assay of bacterial pathogens based on Co_3O_4 magnetic nanozymes conjugated with specific fusion phage proteins and magnetophoretic chromatography. ACS Appl. Mater. Interfaces **12**(8), 9090–9097 (2020)

27. Liu, C., Cai, Y., Wang, J., Liu, X., Ren, H., Yan, L., Zhang, Y., Yang, S., Guo, J., Liu, A.: facile preparation of homogeneous copper nanoclusters exhibiting excellent tetraenzyme mimetic activities for colorimetric glutathione sensing and fluorimetric ascorbic acid sensing. ACS Appl. Mater. Interfaces **12**(38), 42521–42530 (2020)

28. Han, L., Li, C., Zhang, T., Lang, Q., Liu, A.: Au@Ag heterogeneous nanorods as nanozyme interfaces with peroxidase-like activity and their application for one-pot analysis of glucose at nearly neutral pH. ACS Appl. Mater. Interfaces **7**(26), 14463–14470 (2015)

29. Thomas, A., Fischer, A., Goettmann, F., Antonietti, M., Müller, J.O., Schlögl, R., Carlsson, J.M.: Graphitic carbon nitride materials: variation of structure and morphology and their use as metal-free catalysts. J. Mater. Chem. **18**(41), 4893 (2008)

30. Katsumata, K., Motoyoshi, R., Matsushita, N., Okada, K.: Preparation of graphitic carbon nitride (g-C_3N_4)/WO_3 composites and enhanced visible-light-driven photodegradation of acetaldehyde gas. J. Hazard. Mater. **260**, 475–482 (2013)

31. Jullian, C., Fernandez-Sandoval, S., Celis-Barros, C., Abarca, B., Ballesteros, R., Zapata-Torres, G.: Supramolecular assemblies of phenyl-pyridyl-triazolopyridine and beta-cyclodextrin as sensor of divalent cations in aqueous solution. Carbohydr. Polym. **121**, 295–301 (2015)

32. Xu, Y., Wang, L., Zhou, Y., Guo, J., Zhang, S., Lu, Y.: Synthesis of heterostructure SnO_2/graphitic carbon nitride composite for high-performance electrochemical supercapacitor. J. Electroanal. Chem. **852**, 113507 (2019)

33. Zang, Y., Li, L., Li, X., Lin, R., Li, G.: Synergistic collaboration of g-C_3N_4/SnO_2 composites for enhanced visible-light photocatalytic activity. Chem. Eng. J. **246**, 277–286 (2014)

34. Li, L., Hu, Y., Deng, D., Song, H., Lv, Y.: Highly sensitive cataluminescence gas sensors for 2-butanone based on g-C_3N_4 sheets decorated with CuO nanoparticles. Anal. Bioanal. Chem. **408**(30), 8831–8841 (2016)

35. Singh, J., Kumari, P., Basu, S.: Degradation of toxic industrial dyes using SnO_2/g-C_3N_4 nanocomposites: Role of mass ratio on photocatalytic activity. J. Photochem. Photobiol. A **371**, 136–143 (2019)

36. Yang, S., Gong, Y., Zhang, J., Zhan, L., Ma, L., Fang, Z., Vajtai, R., Wang, X., Ajayan, P.M.: Exfoliated graphitic carbon nitride nanosheets as efficient catalysts for hydrogen evolution under visible light. Adv. Mater. **25**(17), 2452–2456 (2013)

37. Rono, N., Kibet, J.K., Martincigh, B.S., Nyamori, V.O.: A review of the current status of graphitic carbon nitride. Crit. Rev. Solid State Mater. Sci., 1–29 (2020)

38. Ismael, M.: A review on graphitic carbon nitride (g-C_3N_4) based nanocomposites: synthesis, categories, and their application in photocatalysis. J. Alloys Compd. **846**, 156446 (2020)

39. Chen, W., Liu, T.Y., Huang, T., Liu, X.H., Yang, X.J.: Novel mesoporous P-doped graphitic carbon nitride nanosheets coupled with $ZnIn_2S_4$ nanosheets as efficient visible light driven heterostructures with remarkably enhanced photo-reduction activity. Nanoscale **8**(6), 3711–3719 (2016)

40. Zhao, X., Li, S., Yu, X., Gang, R., Wang, H.: In situ growth of CeO_2 on g-C_3N_4 nanosheets toward a spherical g-C_3N_4/CeO_2 nanozyme with enhanced peroxidase-like catalysis: a selective colorimetric analysis strategy for mercury (II). Nanoscale **12**(41), 21440–21446 (2020)

41. Fan, Y., Zhang, W., Liu, Y., Zeng, Z., Quan, X., Zhao, H.: Three-dimensional branched crystal carbon nitride with enhanced intrinsic peroxidase-like activity: a hypersensitive platform for colorimetric detection. ACS Appl. Mater. Interfaces **11**(19), 17467–17474 (2019)

42. Liu, B., Wang, Y., Chen, Y., Guo, L., Wei, G.: Biomimetic two-dimensional nanozymes: synthesis, hybridization, functional tailoring, and biosensor applications. J. Mater. Chem. B **8**(44), 10065–10086 (2020)

43. Siddiqui, A.S., Hayat, A., Nawaz, M.H., Ahmad, M.A., Nasir, M.: Effect of sulfur doping on graphene oxide towards amplified fluorescence quenching based ultrasensitive detection of hydrogen peroxide. Appl. Surf. Sci. **509**, 144695 (2020)

44. She, X., Xu, H., Xu, Y., Yan, J., Xia, J., Xu, L., Song, Y., Jiang, Y., Zhang, Q., Li, H.: Exfoliated graphene-like carbon nitride in organic solvents: enhanced photocatalytic activity and highly selective and sensitive sensor for the detection of trace amounts of Cu^{2+}. J. Mater. Chem. **2**(8), 2563–2570 (2014)

45. Ahmed, A., John, P., Nawaz, M.H., Hayat, A., Nasir, M.: Zinc-doped mesoporous graphitic carbon nitride for colorimetric detection of hydrogen peroxide. ACS Appl. Nano Mater. **2**(8), 5156–5168 (2019)

46. Mu, J., Li, J., Zhao, X., Yang, E.-C., Zhao, X.-J.: Cobalt-doped graphitic carbon nitride with enhanced peroxidase-like activity for wastewater treatment. RSC Adv. **6**(42), 35568–35576 (2016)

47. Qiao, F., Wang, J., Ai, S., Li, L.: As a new peroxidase mimetics: The synthesis of selenium doped graphitic carbon nitride nanosheets and applications on colorimetric detection of H_2O_2 and xanthine. Sens. Actuators B Chem. **216**, 418–427 (2015)

48. Wu, N., Wang, Y.T., Wang, X.Y., Guo, F.N., Wen, H., Yang, T., Wang, J.H.: Enhanced peroxidase-like activity of AuNPs loaded graphitic carbon nitride nanosheets for colorimetric biosensing. Anal. Chim. Acta **1091**, 69–75 (2019)

49. Song, Y., Qu, K., Zhao, C., Ren, J., Qu, X.: Graphene oxide: intrinsic peroxidase catalytic activity and its application to glucose detection. Adv. Mater. **22**(19), 2206–2210 (2010)

50. Miao, Y.-E., He, S., Zhong, Y., Yang, Z., Tjiu, W.W., Liu, T.: A novel hydrogen peroxide sensor based on Ag/SnO_2 composite nanotubes by electrospinning. Electrochim. Acta **99**, 117–123 (2013)

51. Panagiotopoulos, A., Gkouma, A., Vassi, A., Johnson, C.J., Cass, A.E.G., Topoglidis, E.: Hemin modified SnO_2 films on ITO-PET with enhanced activity for electrochemical sensing. Electroanalysis **30**(9), 1956–1964 (2018)

52. Liu, Y., Wang, L., Yang, L., Zhan, Y., Zou, L., Ye, B.: Nonenzymatic H_2O_2 electrochemical sensor based on SnO_2 NPs coated polyethylenimine functionalized graphene. Electroanalysis **29**(9), 2044–2052 (2017)

53. Liu, S., Yu, B., Li, F., Ji, Y., Zhang, T.: Coaxial electrospinning route to prepare Au-loading SnO_2 hollow microtubes for non-enzymatic detection of H_2O_2. Electrochim. Acta **141**, 161–166 (2014)

54. Kafi, A.K.M., Wali, Q., Jose, R., Biswas, T.K., Yusoff, M.M.: A glassy carbon electrode modified with SnO_2 nanofibers, polyaniline and hemoglobin for improved amperometric sensing of hydrogen peroxide. Microchim. Acta **184**(11), 4443–4450 (2017)

55. Fu, Y., Huang, D., Li, C., Zou, L., Ye, B.: Graphene blended with SnO_2 and Pd-Pt nanocages for sensitive non-enzymatic electrochemical detection of H_2O_2 released from living cells. Anal. Chim. Acta **1014**, 10–18 (2018)

56. Jana, S., Mondal, A.: Fabrication of SnO_2/alpha-Fe_2O_3, SnO_2/alpha-Fe_2O_3-PB heterostructure thin films: enhanced photodegradation and peroxide sensing. ACS Appl. Mater. Interfaces **6**(18), 15832–15840 (2014)

57. Samourgkanidis, G., Nikolaou, P., Gkovosdis-Louvaris, A., Sakellis, E., Blana, I.M., Topoglidis, E.: Hemin-modified SnO_2/Metglas electrodes for the simultaneous electrochemical and magnetoelastic sensing of H_2O_2. Coatings **8**(8), 284 (2018)

58. Chauhan, S., Sahoo, S., Satpati, A.K., Sharma, C., Sahoo, P.K.: Prussian blue nanocubes-SnO_2 quantum dots-reduced graphene oxide ternary nanocomposite: An efficient non-noble-metal electrocatalyst for non-enzymatic detection of H_2O_2. Electroanalysis **32**(8), 1763–1771 (2020)

59. Lavanya, N., Radhakrishnan, S., Sekar, C.: Fabrication of hydrogen peroxide biosensor based on Ni doped SnO_2 nanoparticles. Biosens. Bioelectron. **36**(1), 41–47 (2012)

60. Ding, Y., Yang, B., Liu, H., Liu, Z., Zhang, X., Zheng, X., Liu, Q.: FePt-Au ternary metallic nanoparticles with the enhanced peroxidase-like activity for ultrafast colorimetric detection of H_2O_2. Sens. Actuators B Chem. **259**, 775–783 (2018)

61. Zhang, Q., Li, M., Guo, C., Jia, Z., Wan, G., Wang, S., Min, D.: Fe_3O_4 nanoparticles loaded on Lignin nanoparticles applied as a peroxidase mimic for the sensitively colorimetric detection of H_2O_2. Nanomaterials (Basel) **9**(2), 210 (2019)

62. Qiao, F., Qi, Q., Wang, Z., Xu, K., Ai, S.: MnSe-loaded g-C_3N_4 nanocomposite with synergistic peroxidase-like catalysis: Synthesis and application toward colorimetric biosensing of H_2O_2 and glucose. Sens. Actuators B Chem. **229**, 379–386 (2016)

63. Sun, J., Li, C., Qi, Y., Guo, S., Liang, X.: Optimizing colorimetric assay based on V_2O_5 nanozymes for sensitive detection of H_2O_2 and glucose. Sensors (Basel) **16**(4), 584 (2016)

64. Lu, J., Zhang, H., Li, S., Guo, S., Shen, L., Zhou, T., Zhong, H., Wu, L., Meng, Q., Zhang, Y.: Oxygen-vacancy-enhanced peroxidase-like activity of reduced Co_3O_4 nanocomposites for the colorimetric detection of H_2O_2 and glucose. Inorg. Chem. **59**(5), 3152–3159 (2020)

65. Liu, S., Tian, J., Wang, L., Luo, Y., Sun, X.: A general strategy for the production of photoluminescent carbon nitride dots from organic amines and their application as novel peroxidase-like catalysts for colorimetric detection of H_2O_2 and glucose. RSC Adv. **2**(2), 411–413 (2012)

66. Chen, J., Chen, Q., Chen, J., Qiu, H.: Magnetic carbon nitride nanocomposites as enhanced peroxidase mimetics for use in colorimetric bioassays, and their application to the determination of H_2O_2 and glucose. Microchim. Acta **183**(12), 3191–3199 (2016)

67. Ju, P., He, Y., Wang, M., Han, X., Jiang, F., Sun, C., Wu, C.: Enhanced peroxidase-like activity of MoS_2 quantum dots functionalized g-C_3N_4 nanosheets towards colorimetric detection of H_2O_2. Nanomaterials (Basel) **8**(12), 976 (2018)

Authors and Affiliations

Aftab Ahmed[1,2] · Akhtar Hayat[1] · Peter John[2] · Mian Hasnain Nawaz[1] · Muhammad Nasir[1]

[1] Interdisciplinary Research Centre in Biomedical Materials (IRCBM), COMSATS University Islamabad, Lahore Campus, 1.5 Km Defence Road, off Raiwind Road, Lahore 54000, Punjab, Pakistan

[2] Government College University Lahore, Katchery Road, Anarkali, Lahore 54000, Punjab, Pakistan